



NOVA

University of Newcastle Research Online

nova.newcastle.edu.au

Berriman, G.; Routley, B.; Clothier, S.; Holdsworth, J. L.; Belcher, W. J.; Zhou, X. J.; Dastoor, P. C. "Development of a multi-wavelength photocurrent mapping system". Originally published in Measurement Science and Technology Vol. 24, Issue 10 (2013)

Available from: <http://dx.doi.org/10.1088/0957-0233/24/10/105604>

This is an author-created, un-copyedited version of an article accepted for publication in Measurement Science and Technology. IOP Publishing Ltd is not responsible for any errors or omissions in this version of the manuscript or any version derived from it. The definitive publisher authenticated version is available online at 10.1088/0957-0233/24/10/105604

**Accessed from:** <http://hdl.handle.net/1959.13/1061729>

## Development of a multi-wavelength photocurrent mapping system.

G Berriman, B Routley, S Clothier, J Holdsworth\*, W Belcher, X Zhou, P Dastoor

<sup>1</sup>*Centre for Organic Electronics, University of Newcastle, Callaghan, NSW 2308, Australia*

\*E-mail: John.Holdsworth@newcastle.edu.au

### Abstract

A novel multi-wavelength near-field scanning photocurrent microscopy (MWNSPM) system has been developed, which directly correlates photocurrent generation at different incident wavelengths with morphology of organic photovoltaic (OPV) cells. The system is based on a near-field scanning optical microscope (NSOM) which generates the topographical map and acts as the nano-scale light source for the OPV cell. The light sources are frequency modulated using optical beam choppers, and the resulting photocurrent signal is demodulated in software via a Fourier transform to recover the signal due to each wavelength. A spatial resolution of  $170 \pm 45$  nm was achieved, in good agreement with the probe aperture, using a poly(9,9'-dioctylfluorene-co-bis-N,N'-(4-butylphenyl)-bis-N,N'-phenyl-1,4-phenylene-diamine) [PFB] and poly(9,9'-dioctylfluorene-co-benzo-thiadiazole) [F8BT] OPV device.

**Keywords:** Photocurrent map, Organic photovoltaic cell, Conductive polymer, Near-field scanning optical microscopy (NSOM)

(Some figures in this article are in colour only in the electronic version)

## 1. Introduction

Conducting polymer photovoltaic devices hold great promise as an alternative to silicon for harnessing of solar energy due to the potential for fabrication *via* cheap, well-established polymer production and processing techniques [1–3]. The active layer of the devices is generally composed of two or more materials sandwiched between a semi-transparent anode and a metal cathode, although other architectures are possible [4,5]. A bulk heterojunction active layer is most commonly used, which is formed by blending the solvated organic components and then depositing the film onto a substrate/electrode by spin casting or any number of printing techniques [2,6].

During the coating process or subsequent thermal annealing steps, the materials begin to phase separate resulting in a complex 3D interpenetrating structure [7]. The resulting domain sizes and their composition, position, orientation and location relative to the electrodes have a great influence on how well the device will perform and significant advances in device performance have been achieved by tailoring the deposition and annealing steps to generate the most favourable microstructure and hence photocurrent [8–10].

Despite rapid advances in the understanding of the structure-function relationship in OPV devices, relatively little information is known about the correlation between morphology and photocurrent generation. Conventionally, only the bulk performance of an OPV device, averaged over the entire device, is recorded while the morphology of the device is determined using techniques such as electron diffraction, scanning transmission x-ray microscopy (STXM), transmission electron microscopy (TEM) and atomic force microscopy (AFM) [9,11]. In many instances the morphology measurements are carried out on separate films due to constraints

with the measuring equipment and technique. Since the active layer is a heterogeneous blend, there is no reason to expect that the photo-current generated will be uniform across the device, and therefore all the imaging and surface analysis techniques mentioned above fail to identify directly the morphological features or crystal structure responsible for any device enhancement and/or deterioration. Thus, it is possible that the majority of the photocurrent generated in a device arises at favourable morphological features while the rest of the film generates proportionately less and such differences cannot be picked up by conventional approaches.

The first direct photocurrent mapping of organic solar cells was achieved at the University of Newcastle with the use of a modified near-field scanning optical microscope (NSOM) capable of simultaneously generating an AFM height image and a single wavelength induced photocurrent across the mapped region [12]. The resolution was limited by the light field to hundreds of nanometers, which, however seemed to be sufficient for the morphology of many common device films. Subsequently, photoconductive AFM (pc-AFM) has been used to correlate device morphology with photocurrent generation with resolution on the order of 20nm [13], the anticipated diffusion length of the exciton. However, pc-AFM is not ideal as it does not utilise a complete device structure to perform the measurement. In particular, devices used for pc-AFM measurements lack a top metal electrode. The electrode is known to create interface energy states within real devices as well as spreading the electric field across the active layer which plays an important role in charge separation and migration to the electrodes [14]. More recently, confocal microscopy has been used in photocurrent mapping of OPV devices at a number of wavelengths [15]. However, the resolution of this technique is limited by size of the

diffraction limited spot,  $1.22\lambda_{\text{illumination}}$ , effectively just sub-micron. Furthermore, this technique is only able to acquire photocurrent maps sequentially at each wavelength.

Here we report the development of a multi-wavelength near-field scanning photocurrent microscopy (MWNSPM) system. The new system is capable of mapping both the photocurrent at several wavelengths and the topology of the surface all simultaneously via a custom-built demodulation system. We show that the new instrument features an improved resolution, by a factor of 4 – 5 times when compared with previously reported NSPM systems, and show that the apparatus can determine directly which morphology in the device is generating the photocurrent.

## **2. Experimental**

### *2.1 NSOM configuration*

The NSPM technique has been described elsewhere in detail [12] and is summarised for context here. The technique relies on a near-field scanning optical microscope probe to illuminate the photovoltaic cell. The tapered optical fibre tips available feature aperture sizes from 50nm to 500nm, which are below or comparable to the wavelength of visible light and, when positioned within one wavelength of the surface, illuminate the surface in the optical near-field. A height feedback and control system keeps the tip of the probe uniformly above the surface *via* a cantilever and optical lever responding to the atomic force. Maintaining the aperture in the near-field region ensures that the illumination spot diameter is equal in size to the probe aperture, and provides resolution well below the Rayleigh diffraction limit. The sample is raster scanned in the X-Y plane below the fibre tip aperture with the device

photocurrent generated under the illuminated spot recorded for each X-Y position, while the AFM feedback maintains the tip-surface separation and generates a topographical map of the surface. The piezo-electric scanner employed allows X-Y scans as large as 80x80 $\mu\text{m}$  with a maximum Z range of 2 $\mu\text{m}$ .

## *2.2 Multi-wavelength NSOM configuration*

Multiple wavelengths from different lasers were combined using a series of dichroic filters and mirrors to coaxially couple into the NSOM probe fibre using an achromatic microscope objective. Suitable wavelengths must all be capable of being coupled into the same fibre simultaneously and have sufficient transmission through the probe aperture. In practice, it was found that this was possible for wavelengths in the band  $\sim 400\text{-}650\text{nm}$ . A unique issue arises from the choice of probe employed. The probes have a curve in the fibre associated with the taper to the tip and are clad with metal to confine the mode field within the fibre. This metal heats when the illuminating wavelengths are coupled [16] with the undesirable effect that the tip flexes and may illuminate a different spatial position in the X-Y plane unless thermally equilibrated prior to scanning. When coupling multiple wavelengths in a time sequence using shutters to control individual wavelengths, this tip flex becomes difficult to manage as it requires equivalent heat absorption in the metal for each wavelength employed, therefore precise independent control over power coupled for each wavelength. The shutter transition time is in the millisecond time domain and this is of the same order as the tip heating and flexure time constant.

An approach was developed to avoid this problem altogether and has the added benefit of aiding signal detection. Each illuminating wavelength was modulated, by using an optical beam chopper or directly modulating the laser diode, at a separate, unique 100Hz-1kHz frequency, chosen so that the period is shorter than the time constant of tip flexure. This approach avoided the gross tip flexure previously experienced and relaxed the requirement that the power of each of the lasers had to be separately adjustable and balanced. The requirement for tip stability became that the integrated power transiting the tip was constant within the time constant of tip flexure. Figure 1 provides a schematic of the functioning instrument and the representative signal obtained from each illuminating modulated wavelength.

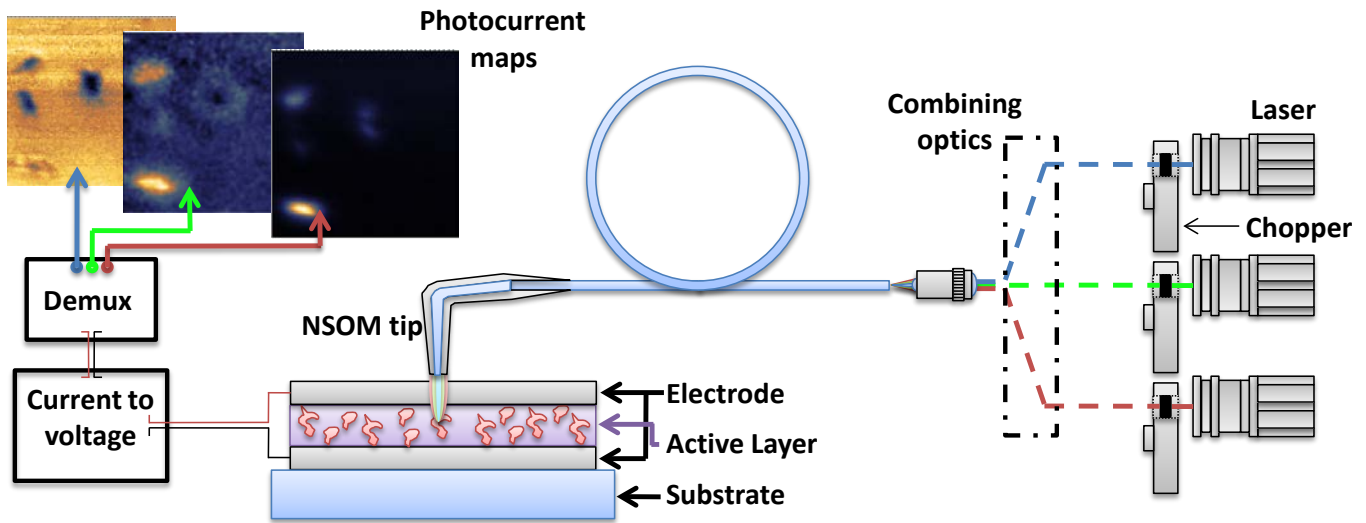


Figure 1: Schematic diagram of the NSPM experimental arrangement. The tapered optical fibre tip acts as both a light source and an AFM tip. The system raster scans the device under the tip and records both photocurrent and topographical maps of the device surface. The metal cathode on the device is semi-transparent.

### *2.3 Signal detection and demodulation*

Each wavelength was modulated at its own unique frequency and multiplexed into the optical fibre probe illuminating the photovoltaic device. These wavelengths excite the device to produce a photocurrent in proportion to the unique absorption of that wavelength in the device and at the modulation frequency of the individual wavelengths. The detected multiplexed photocurrent signal was then filtered and amplified. Capacitive filtering was implemented to remove the DC component of the signal arising from scatter of the feedback laser (used to maintain the tip-surface distance) reflecting from the cantilever. The nA current signal detected from a  $\sim 10^{-19} \text{ m}^3$  excited volume was then passed through a current pre-amplifier which converted the signal to a voltage and amplified it by several orders of magnitude.

The analogue signal was then digitised with a 16 bit National Instruments (NI) data acquisition card (DAQ) located in a NI PXI crate where the signal was demodulated using software written in Labview. The demodulation is accomplished by converting the signal to the Fourier domain and integrating the signal over an appropriate bandwidth, manually selected by the user, for each frequency as shown in Figure 2.

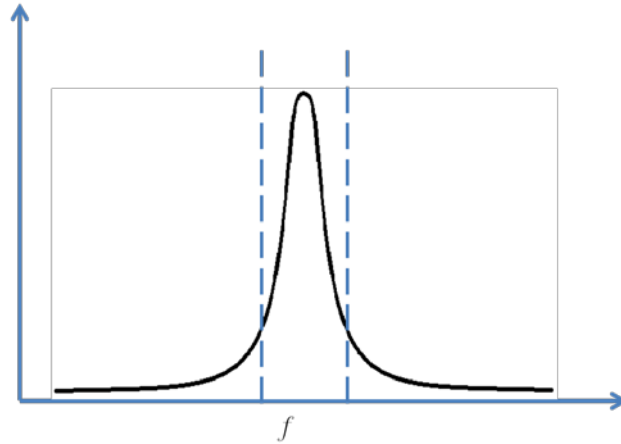


Figure 2: The frequency components of the input signal are extracted by integrating over a user defined frequency range (the dashed vertical lines) in Fourier space. This integration is done manually for each input wavelength and associated modulation frequency.

This system is capable of demodulating an arbitrary number of signals simultaneously within the following practical considerations. The modulation frequencies need to be unique for each wavelength and sufficiently separated so that the individual signals can be resolved in frequency space. The resolution of the frequency space is in turn determined by the number of samples collected at each point in the scan along with the sampling frequency and is given by  $\Delta f = f_s / N$ , where  $f_s$  is the sampling frequency and  $N$  is the number of samples collected. For good signal demodulation, the sampling frequency needs to be well above the Nyquist rate for the highest modulation frequency. In addition, the modulation frequencies need to be low enough to ensure that the photocell is still able to respond rapidly and should also be far from any noise signals. The visualisation of the signal in Fourier space enables the user to select appropriate modulation frequencies so that there is a clearly resolved peak with sufficient amplitude and no

identifiable distortion. This approach does not need individual phase-locked loop detection via lock-in amplifiers, though arguably, a greater signal to noise ratio would be possible with a dedicated lock-in for each wavelength employed. In practice, the PXI crate's ability to demodulate the signal and move the sample stage limited the scan speed to around 2.5 pixels per second.

#### *2.4 Testing the system*

To test the NSPM system on an organic photovoltaic cell (OPV), a device was made using a 1:1 blend of poly(9,9'-dioctylfluorene-co-bis-N,N'-(4-butylphenyl)-bis-N,N'-phenyl-1,4-phenylene-diamine) [PFB] and poly(9,9'-dioctylfluorene-co-benzo-thiadiazole) [F8BT]. The materials were dissolved in p-xylene at a concentration of 25 mg/ml and spin coated onto an indium-tin-oxide (ITO) electrode. A semi-transparent cathode of 10 nm of calcium and 20 nm of silver was deposited on top of the film to complete the device. The wavelengths used to probe the device were 405 nm and 488 nm. Additionally, the active layer was mapped using an Asylum Cypher atomic force microscope to ensure there was agreement with the NSPM system.

### **3. Results and Discussion**

Figure 3 shows the UV-vis absorption spectra of PFB, F8BT and the 1:1 PFB:F8BT blend. The PFB and F8BT absorption spectra are complementary, with incident light at 488nm absorbed primarily by the F8BT component in the film whereas light at 405 nm is absorbed by both the

PFB and F8BT components [15]. As such, photocurrent generated at 488 nm arises from light that is just absorbed by the F8BT component whereas photocurrent generated at 405 nm arises from light that is absorbed by both components.

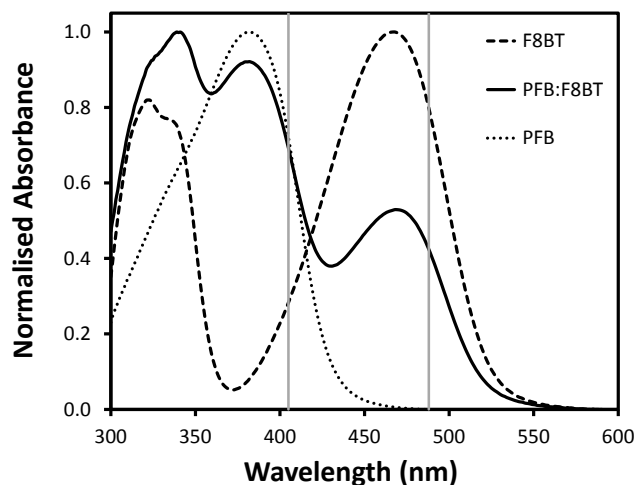


Figure 3: Absorption spectra for PFB, F8BT and a 1:1 blend of the two. The 488nm light is absorbed primarily by the F8BT.

Previous work in this laboratory and by others has shown the PFB:F8BT 1:1 blends in xylene form a complex phase segregated morphology comprising of a hierarchy of domains ranging from the micro- through to the nanoscale [17]. Figure 4 shows an AFM image of the as-spun surface and shows that micron size phase segregated cylindrical islands are indeed observed, which in turn contain smaller nano-scaled domains consistent with previous studies [18]. The AFM data also shows that for these samples, the observed circular micron sized domains are thicker than the surrounding blend matrix, rather than thinner as has been observed previously [19] and which most likely arises from differences in molecular weight of the polymer components in the two studies. Notwithstanding these slight variations in surface morphology,

the formation of this hierarchy of domain structures makes these PFB:F8BT blends an ideal test bed for the new MWNSPM system.

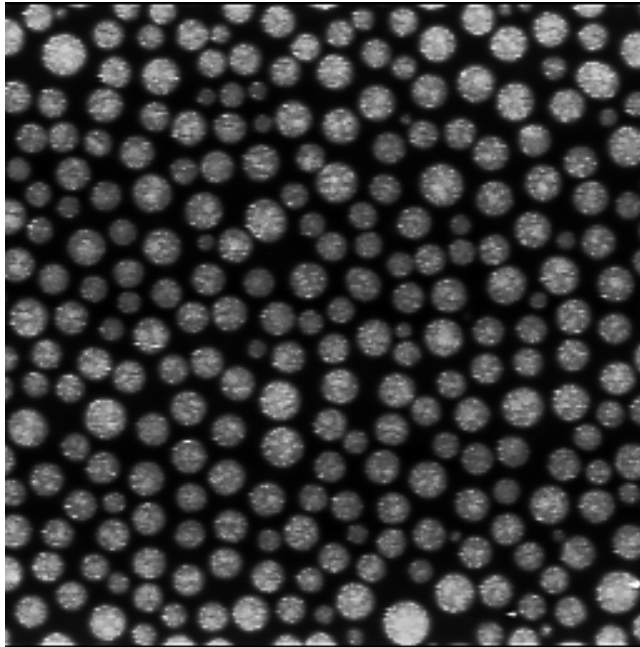


Figure 4: 20  $\mu\text{m}$  x 20  $\mu\text{m}$  AFM image of the 1:1 PFB:F8BT blend film spun from xylene as measured by an Asylum Cypher AFM. The greyscale corresponds to a maximum height difference of 80 nm.

Figure 5 shows the NSPM maps collected at 405 nm and 488 nm together with the associated AFM image collected using the NSPM fibre-optic tip. The photocurrent produced by the 488 nm light is generated mainly in the matrix regions between the micron-sized circular domains indicating that these areas are F8BT-rich, since only F8BT absorbs at this wavelength. This result is consistent with previous compositional mapping of these systems using scanning X-ray transmission microscopy, which show that the F8BT composition in these regions is > 90 % [17]. Moreover, as expected, we see that the photocurrent produced by the 405 nm light is correlated with the photocurrent generated at 488 nm, albeit with a lower absolute magnitude,

consistent with previous confocal/photocurrent microscopy of these blends [15]. The correlation between the two photocurrent distributions is highlighted in Figure 5D, which shows the overlay of the photocurrent maps generated at 405 nm and 488 nm.

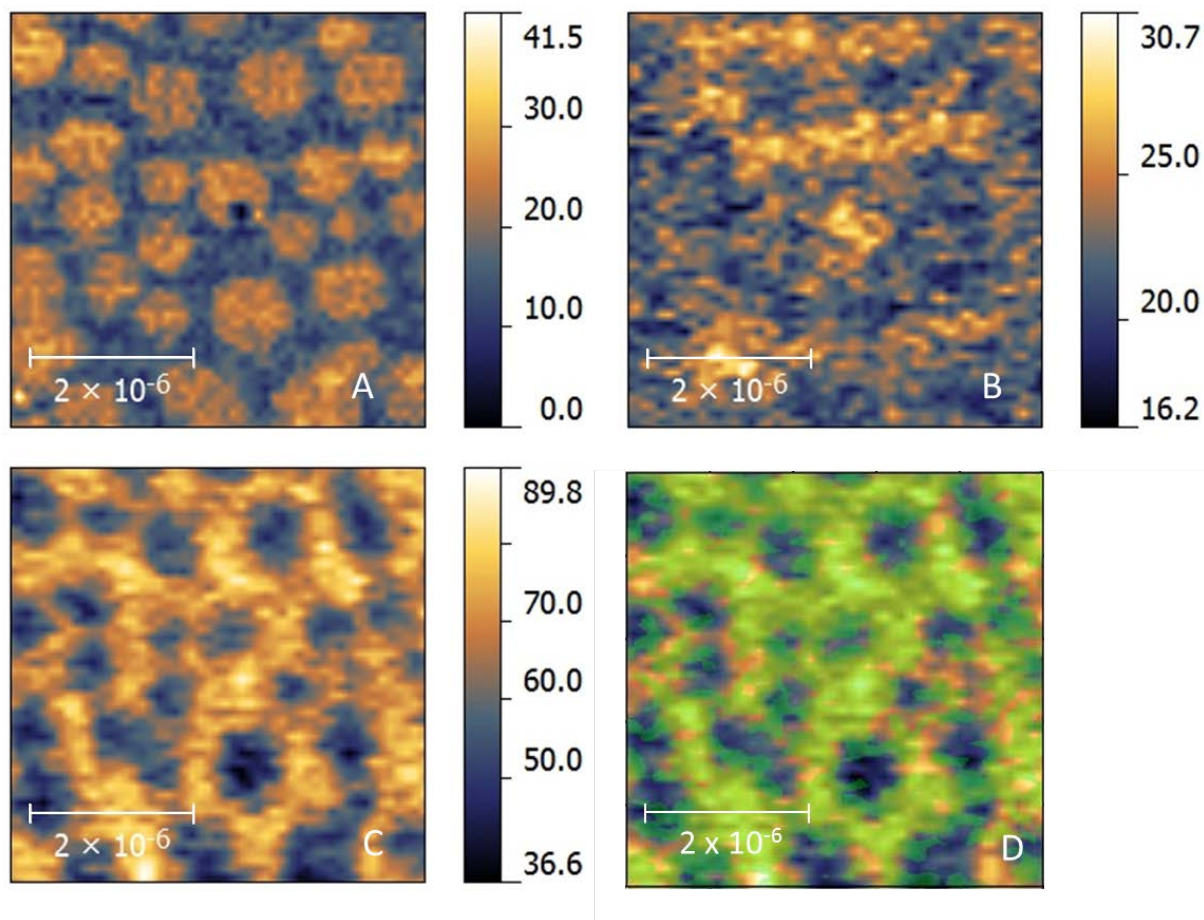


Figure 5: A: Topographical map obtain using the fibre-optic tip of the MWNSPM system with the z axis in nm. B: Photocurrent map generated by incident light of wavelength 405 nm, colour map in nA. C: Photocurrent map generated by incident light of wavelength 488 nm. D: Overlay of the 405 nm (in green) and 488 nm photocurrent maps showing the correlation between the two images.

The resolution of the MWNSPM technique is illustrated in Figure 6, which shows the cross-sectional photocurrent profiles for the original single wavelength NSPM technique [12] compared with the new MWNSPM technique presented here. For both photocurrent profiles a number of edges can be identified (where the profile crosses the edge of a PFB-rich circular micron-sized domain). The width of these edges (as defined by the regions (solid red lines in Figure 6) where the intensity lies between 10 % and 90 % of the magnitude of the edge signal) has been calculated and averaged over at least 5 edges. The average photocurrent edge width using the new MWNSPM technique is  $170 \pm 45$  nm, which is in good agreement with the 200 nm tip aperture used for the experiments. Furthermore, this measured edge width is significantly lower than the value of  $800 \pm 150$  nm obtained for the average photocurrent edge width using the original single wavelength NSPM technique. This edge width provides a measure of the resolution of the present photocurrent imaging technique and reveals that it is considerably higher than the resolution (700 nm) of confocal photocurrent mapping [15].

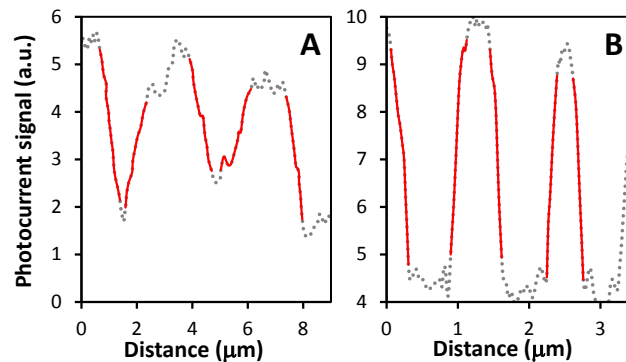


Figure 6: Cross-sectional profiles of the photocurrent maps for incident light of wavelength 488 nm. A: original single wavelength NSPM technique [12]. B: new multi-wavelength NSPM technique. The broken line shows the photocurrent as a function of distance across the whole

profile. The solid red lines identify the profile regions that lie between the 10 % and 90 % threshold limits which are used to define the width of the photocurrent edges.

### **3. Conclusions**

In this paper a novel approach to multi-wavelength near-field scanning photocurrent microscopy (MWNSPM) has been presented, detailing a technique for directly correlating the morphology of an OPV active layer with device function. The new MWNSPM system is capable of measuring the device performance at multiple wavelengths simultaneously all on a single DAQ, thereby negating the need to have a lock-in amplifier for each wavelength. The MWNSPM system's performance was demonstrated on a test sample fabricated from a 1:1 blend of PFB:F8BT, which is known to produce a hierarchy of photocurrent generating domains from the nano- to the micro-scale and which is also known to show strong correlation between morphology and performance. The photocurrent maps that were produced were in good agreement with previous photocurrent mapping work on this system. Moreover, the new MWNSPM system shows considerably improved resolution over existing near-field and confocal photocurrent mapping approaches.

## References

- [1] Brabec C 2004 Organic photovoltaics: technology and market *Solar Energy Materials and Solar Cells* **83** 273
- [2] Krebs F C 2009 Fabrication and processing of polymer solar cells: A review of printing and coating techniques *Solar Energy Materials and Solar Cells* **93** 394–412
- [3] Vak D, Kim S-S, Jo J, Oh S-H, Na S-I, Kim J and Kim D-Y 2007 Fabrication of organic bulk heterojunction solar cells by a spray deposition method for low-cost power generation *Applied Physics Letters* **91** 081102
- [4] Liu J, Namboothiry M a. G and Carroll D L 2007 Fiber-based architectures for organic photovoltaics *Applied Physics Letters* **90** 063501
- [5] Kim J Y, Lee K, Coates N E, Moses D, Nguyen T-Q, Dante M and Heeger A J 2007 Efficient tandem polymer solar cells fabricated by all-solution processing. *Science (New York, N.Y.)* **317** 222–5
- [6] Chang C, Pai C, Chen W and Jenekhe S 2005 Spin coating of conjugated polymers for electronic and optoelectronic applications *Thin Solid Films* **479** 254–60
- [7] Klimov E, Li W, Yang X, Hoffmann G G and Loos J 2006 Scanning near-field and confocal Raman microscopic investigation of P3HT–PCBM systems for solar cell applications *Macromolecules* **39** 4493–6
- [8] Yang X and Loos J 2007 Toward high-performance polymer solar cells: the importance of morphology control *Macromolecules* **40** 1353–62
- [9] Hoppe H, Niggemann M, Winder C, Kraut J, Hiesgen R, Hinsch A, Meissner D and Sariciftci N S 2004 Nanoscale morphology of conjugated polymer/fullerene-based bulk-heterojunction solar cells *Advanced Functional Materials* **14** 1005–11
- [10] Janssen G, Aguirre A, Goovaerts E, Vanlaeke P, Poortmans J and Manca J 2007 P HYSICAL J OURNAL Optimization of morphology of P3HT / PCBM films for organic solar cells : effects of thermal treatments and spin coating **290** 287–90
- [11] Yang X, Loos J, Veenstra S C, Verhees W J H, Wienk M M, Kroon J M, Michels M a J and Janssen R a J 2005 Nanoscale morphology of high-performance polymer solar cells. *Nano letters* **5** 579–83

- [12] McNeill C R, Frohne H, Holdsworth J L, Furst J E, King B V and Dastoor P C 2004 Direct photocurrent mapping of organic solar cells using a near-field scanning optical microscope *Nano Letters* **4** 219–23
- [13] Coffey D C, Reid O G, Rodovsky D B, Bartholomew G P and Ginger D S 2007 Mapping local photocurrents in polymer/fullerene solar cells with photoconductive atomic force microscopy. *Nano letters* **7** 738–44
- [14] Godlewski J 2005 Currents and photocurrents in organic materials determined by the interface phenomena. *Advances in colloid and interface science* **116** 227–43
- [15] Brenner T J K and McNeill C R 2011 Spatially resolved spectroscopic mapping of photocurrent and photoluminescence in polymer blend photovoltaic devices *The Journal of Physical Chemistry C* **115** 19364–70
- [16] Gucciardi P G, Colocci M, Labardi M and Allegrini M 1999 Thermal-expansion effects in near-field optical microscopy fiber probes induced by laser light absorption *Applied Physics Letters* **75** 3408
- [17] McNeill C R, Watts B, Thomsen L, Ade H, Greenham N C and Dastoor P C 2007 X-ray microscopy of photovoltaic polyfluorene blends: relating nanomorphology to device performance *Macromolecules* **40** 3263–70
- [18] McNeill C R, Watts B, Thomsen L, Belcher W J, Greenham N C, Dastoor P C and Ade H 2009 Evolution of laterally phase-separated polyfluorene blend morphology studied by X-ray spectromicroscopy *Macromolecules* **42** 3347–52
- [19] McNeill C R, Frohne H, Holdsworth J L and Dastoor P C 2004 Near-field scanning photocurrent measurements of polyfluorene blend devices: directly correlating morphology with current generation. *Nano Letters* **4** 2503–7